Received February 1998
Revised September 1998
Accepted October 1998

Modelling of heat transfer coupled with columnar dendritic growth in continuous casting of steel

M. M'Hamdi
IRSID, Maizières-lès-Metz, France
H. Combeau and G. Lesoult
Ecole Des Mines de Nancy, Nancy, France

Keywords *Columnar growth, Heat transfer, Modelling, Solidification, Steel*

Abstract *The general aim of this work is to calculate the extent of the equiaxed zone in continuously cast steel products. Free equiaxed grains can grow only in undercooled liquid regions. Undercooling of the bulk liquid occurs because the columnar dendrite tips growing from the mould reject solutes in the liquid. The specific aim of this contribution is to calculate the thermal and physical state of continuously cast steel long products assuming a columnar solidification mode, taking into account the tip undercooling at the solidification front. A 2-D heat transfer model has been developed where the columnar solidification mode is assumed. The calculation of the undercooling at the advancing solidification front is coupled with the heat transfer equation. The comparison between the results of the present model and the classical heat transfer model indicates the importance of modelling the undercooling phenomenon. The influence of the secondary cooling has also been studied.*

1. Introduction

In the case of industrial processes, like continuous casting of steel, the observed structure consists of dendritic crystals. The structure of these crystals can be either columnar or equiaxed. The columnar structure develops from the surface of the product and has a preferred growth axis mainly parallel to the thermal gradient. Due to the columnar dendrite tip undercooling, a region where the local temperature is lower than the liquidus temperature of the bulk liquid is formed ahead of the solidification front. In this zone, free equiaxed grains can grow with independent orientations from each other. As a result of this growth, the columnar-to-equiaxed transition (CET) may occur and form the central equiaxed zone.

The quality of the continuously cast steel depends largely on the process parameters and on the ratio of the columnar to the equiaxed regions. It is known that an equiaxed structure often presents less segregation (Alberny and Birat, 1976) and is generally associated with better quality products. Numerous mathematical and physical models have been developed to understand the transport processes in continuous casting of steel and to predict the influence of various casting parameters (Aboutalebi *et al.*, 1995; Flint, 1990; Huang *et al.*,

International Journal of Numerical Methods for Heat & Fluid Flow, Vol. 9 No. 3, 1999, pp. 296-317.

Financial support from IRSID is gratefully acknowledged.

1992). None of these works, however, takes into account the dendritic growth phenomena. Several works have already dealt with the problem of the columnar-to-equiaxed transition, both numerically and experimentally (Hunt, 1984; Wang and Beckermann, 1994; Vannier, 1994; Jang and Hellawell, 1991), yet only a few of them are directly applicable to the case of continuous casting of steel. Etienne (1990) developed a 1-D heat transfer model for CET prediction in continuous casting of steel where the tip undercooling and growth of the equiaxed grains were taken into account. The effect of undercooling on the thermal state, however, was not discussed. Moreover, such a 1-D model cannot be directly extended for dealing with 2-D or 3-D geometry.

The present work is a preliminary step towards the coupling of the columnar and equiaxed growths in continuous casting of steel and CET prediction. In this study, a 2-D Finite Volume model has been developed in order to calculate the thermal and the physical state of continuously cast steel long products, in which only the columnar solidification is considered. This model couples a classical heat transfer model at the macroscopic scale with a model of microsegregation, which takes into account the dendrite tip undercooling at the microscopic level. Although melt convection is neglected in this study, the formalism introduced here can be extended in order to incorporate convection in the liquid and its effects on the dendrite tip undercooling. The model is applied to a case of continuous casting to indicate the importance of modelling the undercooling phenomenon and to show the difference between the results obtained with a classical heat transfer model and the model we have developed.

2. Heat transfer at the macroscopic scale

The basic difficulty in heat transfer description during solidification in continuous casting of steel is the geometrical complexity of the solid-liquid interface. Figure 1 presents the different regions during solidification in continuous casting. One can distinguish the liquid bulk, the solid region and the mushy zone. It is difficult to solve the heat transfer equation in each region and then to apply the boundary conditions at the interface between the different zones. It is more suitable to apply the general volume averaged conservation equations where the liquid, the mushy zone and the solid are described as a single continuous equivalent medium (Beckermann and Viskanta, 1993; Voller and Prakash, 1987).

2.1 Model assumptions

The two-dimensional (2-D) heat transfer equation is derived on the basis of the following assumptions:

- Heat transfer by convection in the liquid and mushy regions is neglected. The liquid phase moves downwards at the casting velocity.
- The solid phase is rigid and moves downwards at the casting velocity.
- 2-D cartesian and cylindrical geometries are considered.

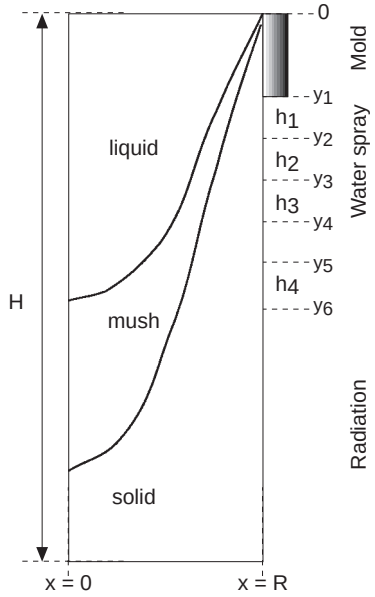

Figure 1.
Solution domain and mould region

- Although the thermophysical properties for solid and liquid phases of steel (c_p, ρ, λ) are dependent of temperature and composition, they were assumed to be constant and equal.

2.2 Governing equations

The governing equations have been derived on the basis of a continuum model for binary alloys, as originally developed by Ganesan and Poirier (1990) and Ni and Beckermann (1991). The heat averaged transport equation can be written as follows:

$$\frac{\partial}{\partial t}(\rho^l g^l h^l + \rho^s g^s h^s) + \vec{\nabla} \cdot (\rho^l g^l h^l \vec{v}^l + \rho^s g^s h^s \vec{v}^s) = \vec{\nabla} \cdot (\lambda \vec{\nabla} T) \tag{1}$$

where λ is the average thermal conductivity of steel:

$$\lambda = g^l \lambda^l + g^s \lambda^s \tag{2}$$

Neglecting the influence of solute, the enthalpies of the liquid and solid phases can be defined as:

$$h^s = \int_{T_0}^{T} c_p^s dT \tag{3}$$

$$h^l = \int_{T_0}^{T} c_p^l dT + L + \int_{T_0}^{T_m} (c_p^s - c_p^l) dT \tag{4}$$

It has been assumed that the reference enthalpy, $h^s(T_0)$, is equal to 0 when $T_0 = 0$. The average density and enthalpy are defined by:

$$\rho = g^l \rho^l + g^s \rho^s \tag{5}$$

$$h = f^l h^l + f^s h^s \tag{6}$$

Moreover, assuming that there is no porosity, one can write:

$$f^s + f^l = 1 \tag{7}$$

$$g^s + g^l = 1 \tag{8}$$

With the simplified assumptions defined in section 2.1, the average enthalpy and the enthalpy for the solid and liquid phases can be written as:

$$h^s = c_p T \tag{9}$$

$$h^l = c_p T + L \tag{10}$$

$$h = c_p T + f^l L \tag{11}$$

The heat averaged transport equation can, thus, be written as:

$$\frac{\partial}{\partial t}(\rho h) + \vec{\nabla} \cdot (\rho h \vec{v}_c) = \vec{\nabla} \cdot (\lambda \vec{\nabla} T) \tag{12}$$

The obtained system of equations consists of five relations (equations 7, 9, 10, 11, 12) and six unknown variables h, h^l, h^s, f^l, $f^s$and T. In order to close this system of equations, it is necessary to establish a supplementary relation. This relation is obtained by considering the solidification phenomena. It is possible, in this way, to relate the solid mass fraction to the temperature such as:

$$f_s = \begin{cases} 0 & \text{if } T > T^*, \\ 1 & \text{if } T < T_s, \\ f_s(T) & \text{if } T_s < T < T^* \end{cases}$$

T^* and T_s are the temperature defining the beginning of solidification and the solidus temperature respectively. The macroscopic heat transfer equation is coupled with a micro-model of columnar growth which is able to describe the solute diffusion at the microscopic level and to determine the temperature defining the beginning of solidification as well as the relation between the temperature and the liquid mass fraction, $f_s(T)$.

3. Micro-model of columnar growth

Figure 2 shows the typical temperature profile for columnar dendritic grains growing from a cooled mould wall towards the centre of a casting. The latent heat of solidification is conducted through the dendrites to the cooled surface. The temperature gradient is imposed by the process and the dendrite tip temperature is primarily controlled by the diffusion of solutes in the liquid ahead of the solidification front and by the condition of thermodynamic equilibrium (Kurz and Fisher, 1989). The movement of the isotherms constrains the dendrite growth velocity which determines the tip undercooling. The interface temperature of the dendrite tip is, then, lower than the equilibrium liquidus temperature of the bulk liquid.

The part of the bulk liquid located ahead of the solidification front, where the temperature is lower than that of the equilibrium liquidus, is referred to as the undercooled zone. In order to model this region, it is necessary to take into account the dendrite tip undercooling. The model that has been used to describe this phenomenon will be presented below.

3.1 Undercooling model

Several theoretical models have been proposed to describe the dendrite tip undercooling (Trivedi, 1980; Kurz and Fisher, 1981). The KGT model by Kurz *et al.* (1986), includes the undercooling that arises from solutal, curvature and kinetic effects and is valid under high growth rates. The proposed micro-model is similar to the KGT model, where only solutal undercooling is considered. For the growth rates in continuous casting, the other effects can be neglected. Although melt convection can influence the dendrite tip growth conditions (Glicksman *et al.*, 1995), its effect was not taken into account in the present study. The specific features of our model of solute diffusion at the microscopic

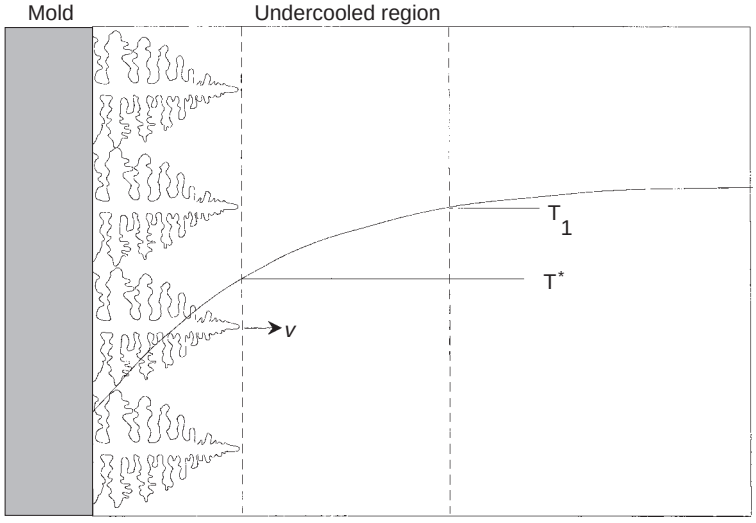

Figure 2.
Columnar solidification

level are based on Ivantsov's (1947) solution for the diffusion field around a paraboloidal dendrite tip and on the marginal stability criterion, generalised to the case of a multicomponent alloy by Bobadilla *et al.* (1988). The dendrite tip undercooling, ΔT^*, which equals the difference between the equilibrium liquidus temperature, associated to the bulk liquid composition, w_i^0, and the dendrite tip interface, T^*, associated to the liquid composition at the dendrite tip, can be expressed in the following way (1988):

$$\Delta T^* = \sum_{i=1}^{n} m_i w_i^0 \left(1 - \frac{1}{1 - (1 - k_i) Iv(P_c^i)}\right) \tag{13}$$

$$P_c^i = \frac{v \cdot r_p}{2D_i^l} \tag{14}$$

$$\Omega_i = \frac{w_i^* - w_i^0}{w_i^* \cdot (1 - k_i)} = Iv(P_c^i) \tag{15}$$

where, Iv, is the Ivantsov function; P_c^i, the solutal Péclet number; v, the interface growth velocity; r_p, the tip radius ; D_i^l, the diffusion coefficient in the liquid phase; k_i, the equilibrium partition ratio and m_i, the liquidus slope. The relation between the supersaturation, Ω_i, the tip composition, w_i^*, and the Péclet number is given by equation (15).

Equation (13) shows that the dendrite tip undercooling depends on the dendrite growth velocity, v, and the dendrite tip radius, r_p. According to the stability criterion developed by Langer and Müller-Krumbhaar (1988), the observed tip radius, r_p, is equal to the shortest wavelength of perturbations, which can develop under the local growth conditions at the tip. Bobadilla *et al.* (1988) proposed an extension of this result to the case of a multicomponent alloy:

$$r_p = 2\pi \sqrt{\frac{\Gamma}{\sum_{i=1}^{n} m_i G_c^i \zeta^i - G}} \tag{16}$$

$$G_c^i = -\frac{v}{D_i^l}(1 - k_i) w_i^* \tag{17}$$

$$\zeta^i = 1 - \frac{2k_i}{2k_i - 1 + \sqrt{1 + \left(\frac{2\pi}{P_c^i}\right)^2}} \tag{18}$$

where G_c^i and G are the composition and temperature gradients respectively, evaluated at the solid-liquid interface in the liquid phase. Γ is the Gibbs-Thomson constant and ζ_i is a stability parameter.

The combination of equations (16, 18) gives a relation such as, $r_p = f(r_p, v, G)$. If the dendrite growth velocity and the thermal gradient are known, this equation can be solved by a substitution method in order to obtain the dendrite tip radius r_p. Then, relation (13) permits the evaluation of the undercooling ΔT^* and hence, that of T^*.

The calculations of G and v, and therefore the dendrite tip undercooling, require the knowledge of the thermal history of the cast product, which can be obtained by the heat transfer model at the macroscopic scale. The calculations made in this study have shown that the influence of the thermal gradient, G, on the determination of the dendrite tip radius, r_p, in equation (16) can be neglected. Therefore, G was set to 0 (equation 16).

It should be noted that although the influence of melt convection was neglected in this model, experimental studies carried out by Glicksman *et al.* (1995) showed that the growth parameters (v, r_p, P_c^i) are influenced by the convective transport and that the Ivantsov solution tends to overestimate the Péclet number as a function of undercooling. Some theoretical attempts have been done to calculate the effect of natural or forced convection (Anath and Gill, 1991; Sekerka *et al.*, 1995; Appolaire *et al.*, 1998). Because of melt convection in continuous casting, our model is likely to overestimate the dendrite tip undercooling.

3.1.1 Calculation of the dendrite growth velocity. The observation of the columnar structure in continuously cast products shows that the dendrites grow from the surface towards the centre of the product with an orientation angle, θ, with the surface of the product as shown in Figure 3. This angle is due to the disorientation of the dendrite tips, which grow mainly in the direction of the thermal gradient, by the effort of fluid flow ahead of the solidification front (Moukassi, 1990).

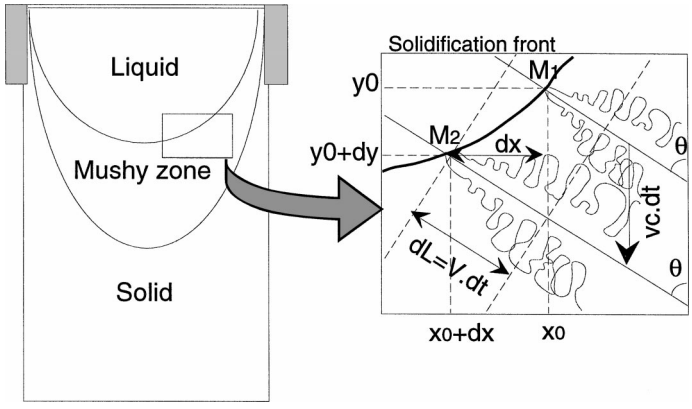

Figure 3.
Dendrite growth direction

As shown by equation (13), in order to determine the dendrite tip undercooling, it is necessary to calculate the dendrite growth velocity, v. This parameter is obtained by determining the position of the dendrite tips ($f_s = 0$). It has been assumed in this study that these positions can be described by a continuous function, ($y = f_t(x)$).

Figure 3 shows a schematic illustration of the solidification front. If the dendrite tip position at time, t, is in M_1, during a time interval, dt, due to the extraction of the product, the dendrite axis is translated by a distance equal to: $dt \cdot v_c$, and the dendrite tip advances to position M_2, as shown in Figure 3.

The dendrite tip advances by distance dL and the dendrite growth velocity is therefore equal to (dL/dt). Given the orientation of the dendrite growth axis, θ, it can be shown that the growth velocity can be written as:

$$v = \frac{v_c}{|cotg(\theta) - \frac{df_t(x)}{dx}|} \sqrt{1 + cotg(\theta)^2} \tag{19}$$

3.2 Solid fraction model

During the solidification of alloys, the latent heat is released over the mushy zone and is related to the evolution of the fraction of solid, $f_s(t)$. In classical heat transfer models, the fraction of solid in the mushy zone is defined as a function of temperature, $f_s(T)$, at the macroscopic level. Depending on the assumption made about the solute diffusion in the solid phase, the relation between the solid fraction and temperature is expressed using the lever rule, Scheil or some back-diffusion model, where solidification begins at the equilibrium liquidus.

To take into account the nonequilibrium conditions at the dendrite tip, it is necessary to couple the undercooling model with the solidification path. The solid fraction model proposed by Flood and Hunt (1987) for a binary alloy uses a Scheil relation truncated at the dendrite tip composition. This approach is easy to implement in a heat transfer model but the solute is not conserved. The model by Giovanola and Kurz (1990) for binary alloys rapid solidification calculations introduces a quadratic polynomial for low fractions of solid whose parameters are calculated to insure solute conservation. McCarthy and Blake (1996) developed a hybrid model of the ones of Flood and Hunt and Giovanola and Kurz, where the solid fraction relationship is truncated at the dendrite tip and solute conservation is assured by imposing the solute flux balance using the method of Giovanola and Kurz.

Kattner *et al.* (1996) proposed an alternate method in order to conserve solute by applying the lever rule at the dendrite tip temperature for the initial alloy composition. This gives the fraction of solid that forms in the tip region and the liquid composition which is equal to the tip composition (if the curvature undercooling is neglected). The obtained liquid composition and the solid fraction are then used as initial values for a solidification path calculated using a Scheil or back-diffusion model. This method can be extended to

multicomponent alloys if the diffusion coefficients in the liquid are taken as identical in the tip undercooling calculation. For unequal values of D_i, this procedure does not conserve solute.

The approach used in the present model is similar to the one proposed by Kattner *et al.* (1996). When the temperature of the dendrite tip is reached, solidification proceeds at a constant temperature, $T = T^*$, until the solid mass fraction is equal to $f^*_{s,i}$, calculated by applying the lever rule to the nominal composition at the temperature T^*.

$$f^*_{s,i} = \frac{w^*_i - w^0_i}{w^*_i \cdot (1 - k_i)} \tag{20}$$

Relation (20) combined with equation (15) gives:

$$f^*_{s,i} = \Omega_i = Iv\left(\frac{v \cdot r_p}{2D_i}\right) \tag{21}$$

This procedure yields to a different value of f^*_i for each solute element. For the remaining solidification path, the calculations are performed using a lever rule or Scheil model with starting values equal to the dendrite tip composition and, f^*_s, the lowest of the fractions of solid $\{f^*_{s,i}\}$:

$$f^*_s = min(\{f^*_{s,i}\}) \tag{22}$$

According to equation (21), relation (22) is met only for the element of solute that has the greatest diffusion coefficient in the liquid phase. For this element, the conservation of mass is assured. For the other solutes, however, our method does not conserve mass and the relative error that we introduce can be expressed in the following way:

$$\frac{\bar{w}_i - w^0_i}{w^0_i} = (1 - k_i)(f^*_{s,i} - f^*_s)\frac{w^*_i}{w^0_i} \tag{23}$$

Equation (23) shows that, except for the solute that diffuses the most in the liquid phase, the effective average solute composition, $\bar{w}_i$, that arises from the assumptions of our method, is always greater than the initial composition for the elements of solute for which k_i is lower than unity. The estimated error that we are making for the alloy used in this study, for the two limiting cases of low and high dendrite growth rates (v=10^{-4} m/s and v=10^{-3} m/s), is given in Table I along with the compositions, partition ratios, diffusion coefficients and liquidus slopes. The relative error is lower that 5 per cent for Silicon and Manganese, while it is high for the elements that have low partition and diffusion coefficients, such as Sulphur and Phosphorus. This should not influence the results given here since these elements are present only in small quantities in the alloy.

For the remaining solidification path, the relation between the solid mass fraction and the liquid composition can be written in the following manner:

- Because of the relatively high back diffusion of carbon in the solid phase within the mushy zone, the lever rule is applied to describe the microsegregation of carbon in the following way:

$$w_i^l = w_i^* \cdot \frac{1-(1-k_i)\cdot f_s^*}{1-(1-k_i)\cdot f_s} \tag{24}$$

- For solutes, which do not diffuse in the solid phase, the Scheil relation is used as follows:

$$w_i^l = w_i^0 \cdot \left(\frac{1-f_s}{1-f_s^*}\right)^{(k_i-1)} \tag{25}$$

Assuming local equilibrium at the interfaces in the mushy zone, the local temperature is related to the solute composition of the liquid phase via the phase diagram by:

$$T = T_f + \sum_{i=1}^{n} m_i \cdot w_i^l \tag{26}$$

Solidification is finished when the solidus temperature, T_s, is reached. To calculate T_s, we used a correlation published by Howe (1988), based on experimental studies. Equations (26), (24) and (25) enable us to determine the $f_s(T)$ relation in the mushy zone as shown in Figure 4.

4. Solution method

Due to symmetry reasons, the calculation domain consists of half of the vertical section of the round product starting at its centre. The spatial discretisation is based on the finite volume method as proposed by Patankar (1980), and the adopted grid system consists of rectangular elements. The governing equation

Solute	C	Si	Mn	S	P
$w_i^0(wt\ pct)$	0.75	0.2	0.65	0.007	0.02
k_i	0.34	0.8	0.79	0.03	0.06
$m_i(K.(wt\ pct)^{-1})$	–62.3	–18.7	–5	–33.5	–33.5
$D_i^l(m^2.s)$	$2\ 10^{-8}$	$3.7\ 10^{-9}$	$3.4\ 10^{-9}$	$2.7\ 10^{-9}$	$3\ 10^{-9}$
Dendrite growth rate: $v = 10^{-4} m/s$					
$f_{s,i}^*$	0.05	0.17	0.13	0.21	0.2
$(\bar{w}_i - w_i^0)/w_i^0$ (per cent)	0	2.4	2.7	18	16
Dendrite growth rate: $v = 10^{-3} m/s$					
$f_{s,i}^*$	0.12	0.33	0.34	0.38	0.36
$(\bar{w}_i - w_i^0)/w_i^0$ (per cent)	0	4.4	4.9	40	34

Table I. Initial liquid composition, partition ratio, liquidus slope, diffusion coefficient, $f_{s,i}^*$, and relative error for each solute element

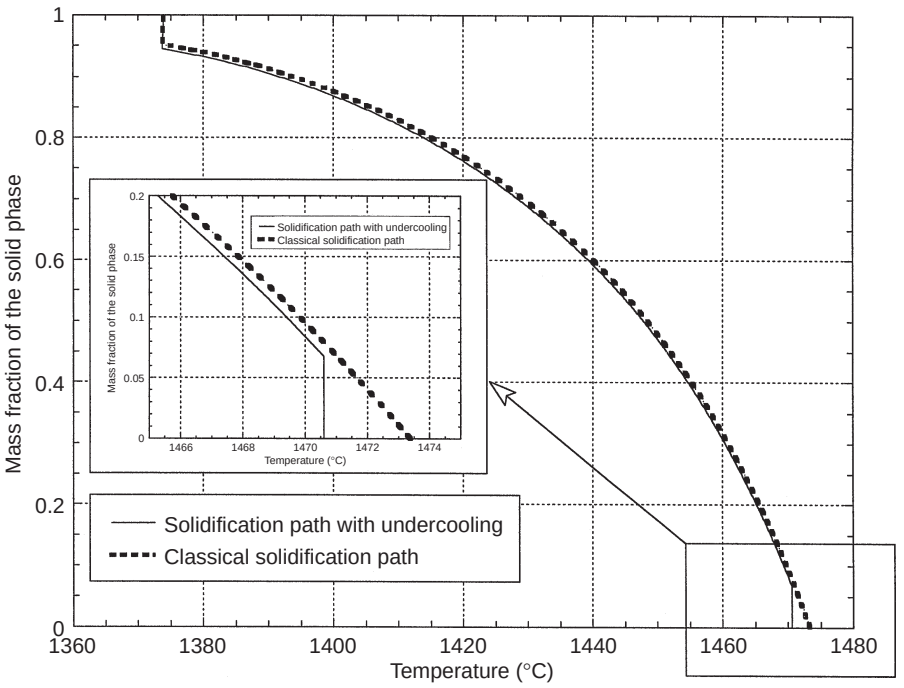

Figure 4.
Comparison between the standard solidification path and the truncated solidification path taking into account the dendrite tip undercooling (Table I): $T_l = 1473.4°C$, $T_s = 1373.9°C$, $T^* = 1470.6°C$

for energy (equation 12) is discretised using a similar approach as proposed in Combeau *et al.* (1990); M'Hamdi *et al.* (1997). The variables (enthalpy, temperature, etc.) are calculated at the main grid points. The Péclet number in the case of continuous casting is sufficiently large. Thus, for the convection term, an upwind scheme was adopted. This procedure yields to a relation such as:

$$a_p h_p + b_p T_p = \sum_{i=1}^{nb} a_i h_i + \sum_{i=1}^{nb} b_i T_i + c \tag{27}$$

where the subscript p is relative to a position in the mesh and nb is the number of neighbouring grid elements. The average enthalpy, h, has been chosen as the main variable for discretisation. For this purpose, the temperature is linearised with a Newton's method:

$$T = T^{\#} + \frac{dT}{dh} \cdot (h - h^{\#}) \tag{28}$$

The symbol $\#$ indicates the best estimated value of a variable. The substitution of the temperature as expressed in equation (28) into equation (27) allows to obtain a relation where the only unknown is the average enthalpy h.

The calculation of (dT/dh) is done by using (11) and $f_s(T)$ relation in the following way:

$$\frac{dT}{dh}\begin{cases} \dfrac{1}{c_p} & \text{if } f_s = 0, \\ \dfrac{1}{c_p} & \text{if } f_s = 1, \\ \dfrac{1}{c_p - L\frac{df_s}{dT}} & \text{if } 0 < f_s < 1. \end{cases}$$

The computation procedure is shown in Figure 5. The calculations start from the steady state solution of classical heat transfer models (i.e. the undercooling at the dendrite tips is not considered and the solidification begins at the equilibrium liquidus temperature). The obtained enthalpy field is, then, an input for the micro-model of columnar growth.

The first step is to calculate the dendrite growth velocity, v. Equation (19) shows that in order to calculate the growth velocity, it is necessary to know the location of the solidification front as a function of x, $f_t(x)$, and its derivative. This function is obtained from the solid mass fraction field. One can see on Figure 6 that the determination of the location of the front from the volume information g_s leads to some error that we have tried to minimise.

In each column of the mesh, the first cell where the solidification front (corresponding to the dendrite tips) is present (i.e. $f_s = 0$), is determined (Figure 6). All these positions are, then, interpolated by a polynomial of Chebyshev ($y = P(x)$). This yields to a continuous function that describes the solidification

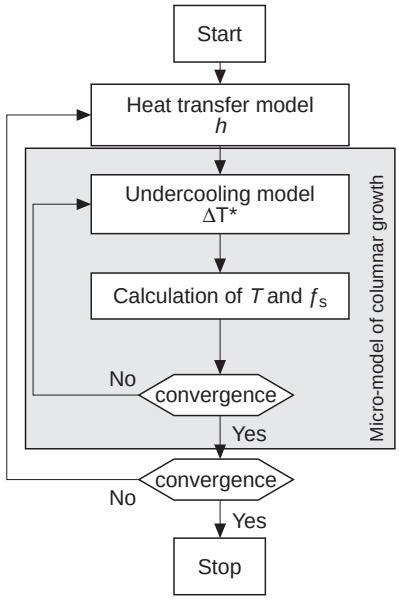

Figure 5.
Resolution algorithm

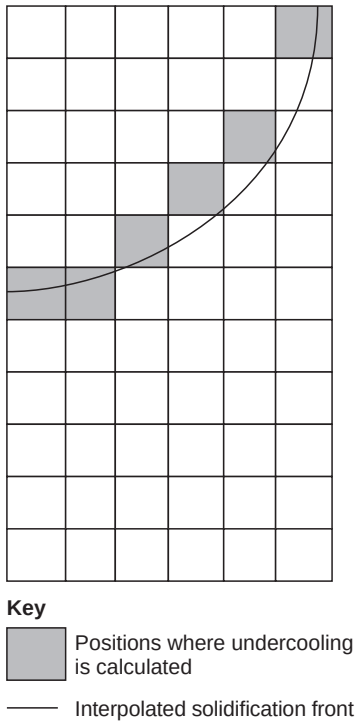

Figure 6.
Interpolation of the positions of the solidification front in the mesh

front and the bulk/mushy zone interface as shown in Figure 6. Assuming, in equation (19), that:

$$\frac{f_t(x)}{dx} = \frac{P(x)}{dx} \tag{29}$$

and restricting the degree of the derivative of $P(x)$ to 3, the dendrite growth velocity can be calculated by equation (19) in the first position of each column of the mesh where the solidification front is present (Figure 6). The dendrite tip undercooling is, then, calculated by the micro-model of columnar growth, and the temperature defining the beginning of solidification is calculated in each column of the mesh. Since the metal moves downwards, and due to the assumption that the solidification front can be described by $(y = f_t(x))$, the solidification path is the same for all positions belonging to the same column. Using equation (11) and the solidification path, the model determines the temperature and the mass fraction fields. This procedure will yield to a new position of the dendrite tips. The calculation of the dendrite tip undercooling modifies the position of the solidification front and the dendrite tip growth velocity, which in its turn modifies the dendrite tip undercooling. An iterative procedure is necessary to solve the non-linear set of equations.

The temperature and the mass fraction fields are then introduced in the heat transfer model (equation (27)). Since the solidification path has been modified, it will yield to new values for (dT/dh). In order to reach the steady state situation, it is necessary to couple the heat transfer model and the micro-model of columnar growth. The discretised equations associated with the appropriate boundary conditions were solved iteratively using a line by line method (Patankar, 1980).

5. Boundary and initial conditions

The liquid surface at the top of the mould constitutes the upper boundary of the calculation domain. Here, temperature across the top surface ($y = 0$) is simply fixed to the casting temperature, T_c, and the liquid metal enters at the casting velocity, v_c. Calculations are performed only in a portion of height, H. This creates an artificial outlet plane down the strand, where the solidified steel leaves the domain. Across this plane, the normal gradient of temperature is set to zero.

Figure 1 shows the boundary conditions along the cooled vertical surface, $x = R$. In the primary cooling region, $y \in [0, y_1]$, a fixed heat flux density, ϕ, is imposed. The secondary cooling consists of four regions, $y \in [y_1, y_2] \cup [y_2, y_3] \cup [y_3, y_4] \cup [y_5, y_6]$. These cooling regions have heat transfer coefficients denoted, h_1, h_2, h_3 and h_4, respectively. The regions in contact with air, the heat flux from the strand surface to the environment takes place by radiation. Hence, for $y \in [y_4, y_5] \cup [y_6, H]$:

$$\frac{\partial T}{\partial y} = \epsilon\sigma \cdot (T^4 - T_{ext}^4) \tag{30}$$

The initial condition at time $t = 0$ is defined as $T(x, y) = T_c$.

6. Modelling examples

The simulation work has been carried out for a multicomponent steel alloy in the case of a round billet caster. The alloy composition, partition ratio and liquidus slope are listed in Table I. The specifications of the continuous casting system and the other thermophysical properties for the used alloy are reported in Table II.

In the first example presented here, the model is applied to a case of continuous casting to indicate the importance of modelling the undercooling phenomenon and to show the difference between the results obtained with a classical heat transfer model and the model we have developed. The calculations have been done considering standard cooling conditions. In the second example, the model is used to study the influence of the secondary cooling on the extent of the undercooled region ahead of the solidification front. For this last example, two calculations were performed. In the first one, a

Symbol	Variable	Value
a_i, a_{nb}, b_i, c	discretisation coefficients	
c_p	specific heat capacity, J.kg^{-1}.K^{-1}	670
c_p^l	specific heat capacity of the liquid phase, J.kg^{-1}.K^{-1}	
c_p^s	specific heat capacity of the solid phase, J.kg^{-1}.K^{-1}	
D_i^l	diffusion coefficient in the liquid, m^{-2}.s	
f^l	liquid mass fraction	
f^s	solid mass fraction	
$f_t(x)$	solidification front interpolation function	
G	thermal gradient, K.m^{-1}	
G_i^c	solutal gradient, wt pct.m^{-1}	
g^l	liquid volumic fraction	
g^s	solid volumic fraction	
h	average mass enthalpy, J.kg^{-1}	
h^l	mass enthalpy of the liquid phase, J.kg^{-1}	
h^s	mass enthalpy of the solid phase, J.kg^{-1}	
I_v	Ivantsov's function	
k_i	equilibrium partition ratio coefficient	
L	latent heat of phase change, J.kg^{-1}	2.5 10^5
m_i	liquidus slope, K.(wt pct)$^{-1}$	
$P(x)$	Chebyshev polynomial	
P_c^i	solutal Péclet number	
r_p	dendrite tip radius, m	
t	time, s	
T_c	casting temperature, ^oC	1490.0
T_l	liquidus temperature, ^oC	1473.4
T_s	solidus temperature, ^oC	1373.9
T^*	temperature of the dendrite tip, ^oC	
T_m	phase-change temperature, ^oC	1528
T_{ext}	ambient temperature, ^oC	20
v_c	casting velocity, m.min^{-1}	0.7
v	dendrite tip growth velocity, m.s^{-1}	
w_i^0	initial solute composition, wt pct	
w_i^*	solute composition at the solid-liquid interface, wt pct	
λ	average conductivity, W.m^{-1}.K^{-1}	30
ρ	density, kg.m^{-3}	7300
ρ^l	density of the liquid phase, kg.m^{-3}	
ρ^s	density of the solid phase, kg.m^{-3}	
ϵ	steel emissivity	1
σ	Stefan-Boltzman constant, W.m^{-2}.K^{-4}	5.667 10^{-8}
Γ	Gibbs-Thomson coefficient, K.m	1.9 10^{-7}
Ω_i	Supersaturation	
ζ	stability constant	
Geometry		
R	Radius, m	0.12
H	Height of solution domain, m	20.0
y_0	distance, m	0.60
y_1	distance, m	0.94
y_2	distance, m	2.46

(continued)

Table II.
Simulation conditions and list of symbols

Symbol	Variable	Value
y_3	distance, m	2.78
y_4	distance, m	3.10
y_5	diatance, m	3.42
Cooling		
ϕ	heat flux in the mould, MW.m^{-2}	1
h_{std1}, h_{sharp1}	heat transfer coefficient, W.m^{-2}.K^{-1}	520.0, 2299.0
h_{std2}, h_{sharp2}	heat transfer coefficient, W.m^{-2}.K^{-1}	362.0, 1045.0
h_{std3}, h_{sharp2}	heat transfer coefficient, W.m^{-2}.K^{-1}	360.0, 360.0
h_{std4}, h_{sharp2}	heat transfer coefficient, W.m^{-2}.K^{-1}	360.0, 360.0

Table II.

standard secondary cooling was applied below the mould region, while in the other one, for the same heat flux in the mould region, a sharp secondary cooling was considered.

The heat transfer coefficients for both standard and sharp secondary coolings (h_{std_i} and h_{sharp_i}) are also listed in Table II. The ambient temperature, T_{ext} is set to 20°C. In all of the cases presented here, the growth direction of the columnar dendrites is considered to be perpendicular to the surface of the product. The employed grid in the mould region consists of 35x50 regular control volumes in the radial and axial directions respectively. For the rest of the computational domain, a grid of 35x205 is used. The number of cells is greater in the mould region where the determination of the solidification front is sensible to the grid size. The calculations were performed until steady-state solution was obtained with a time step of 10s.

6.1 Influence of undercooling on the thermal state

Figures 7 and 8 show the evolution of the calculated dendrite tip undercooling and growth rate respectively along the solidification front. Because of the intense heat transfer in the mould region, near the surface of the product, the dendrites are growing quickly, and high growth rates are obtained. As the dendrites grow towards the centre, the heat transfer is less intense because of the already solidified shell, and the growth rates are smaller.

The undercooling values decrease in the same way as the growth rate and range between 3K and 5K according to the position on the solidification front. The highest values are located close to the surface. Moreover, from the centre of the product to the middle of the radius, the undercooling varies very slightly.

To show the influence of the undercooling on the thermal state, Figures 9a and 10a represent the temperature and liquid mass fraction fields when constitutional undercooling is not considered, while Figures 9b and 10b represent the same fields when the heat transfer calculations take into account the influence of the undercooling at the dendrite tip. The thermal state of the system is modified in the region near the boundary between the liquid bulk and the mushy zone when the dendrite tip undercooling is taken into account. Away from this region, the thermal fields are very similar.

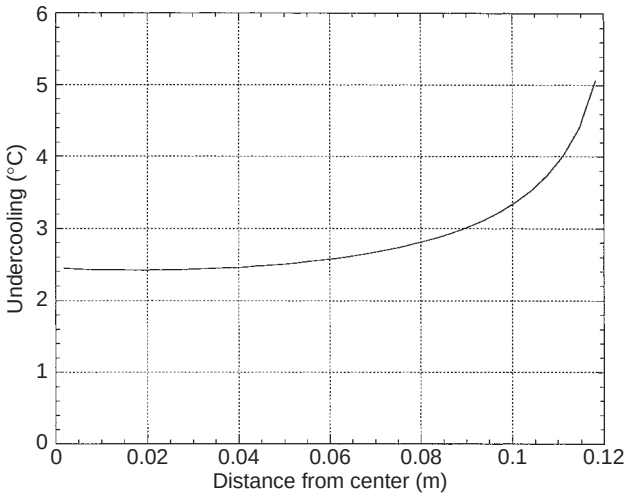

Figure 7.
Dendrite tip undercooling

Figure 10b shows that when undercooling is considered, the position of the solidification front is very different in the region close to the centre than in Figure 10a (no undercooling). The front position is much lower than that obtained with classical heat transfer models. Although the undercooling values are greater close to the surface of the product than in the centre, the influence of the undercooling on the position of the solidification front is much more important in the centre. This is due to the fact that the temperature and solid mass fraction gradients are much lower in the centre than on the surface, so that one degree of undercooling has much more effect on the front position in the centre than near the surface.

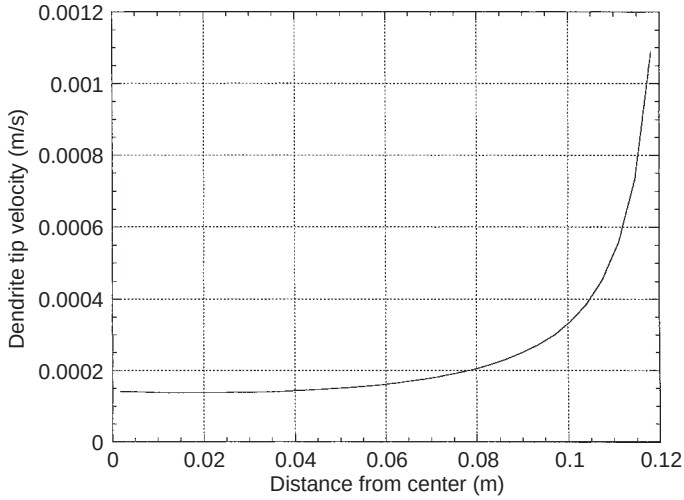

Figure 8.
Dendrite tip velocity

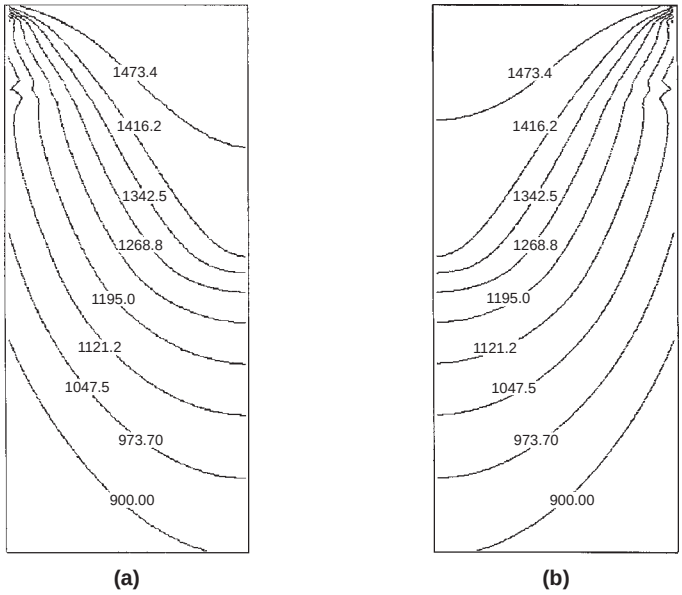

Figure 9.
Temperature field (°*C*): (a) without taking the undercooling into account, (b) with undercooling (T_l: 1473.4°*C*, T_s: 1373.9°*C*, H: 20*m*, R: 0.012*m*)

6.2 Influence of the secondary cooling

Figure 12 shows the dendrite tip undercooling calculated by the model when sharp cooling is applied below the mould region. The heat extraction is higher

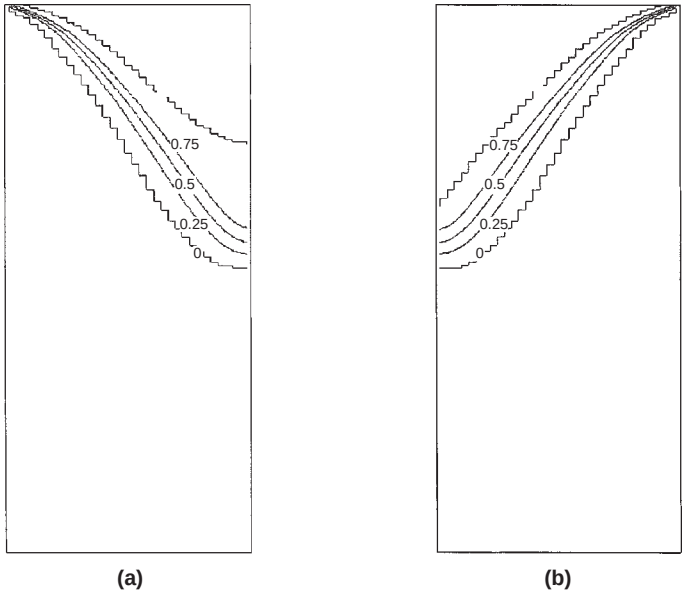

Figure 10.
Liquid mass fraction field: (a) without taking the undercooling into account (b) with undercooling (T_l: 1473.4ºC, T_s: 1373.9ºC, H: 20*m*, R: 0.012*m*)

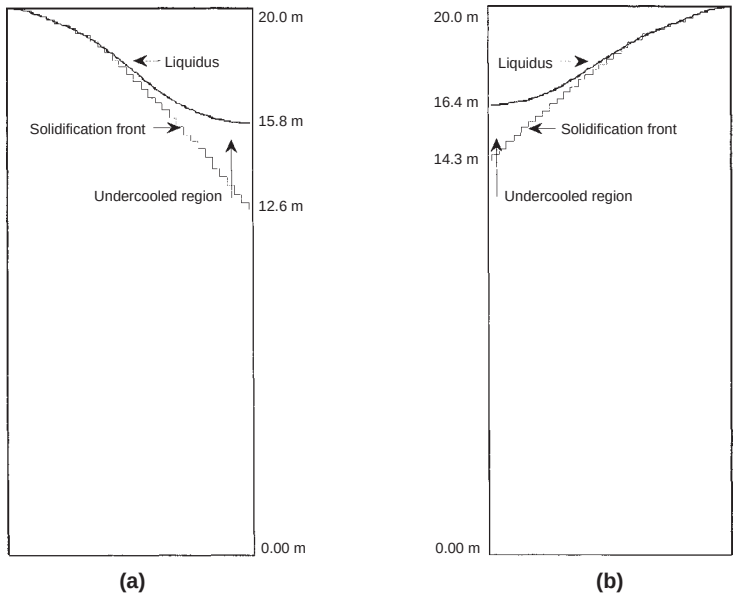

Figure 11.
Undercooled region: (a) standard secondary cooling, (b) sharp secondary cooling (H: 10m, R: 0.012m)

in this case and the dendrite tips advance quicker than with standard cooling. The undercooling values are, therefore, slightly higher with sharp cooling.

In order to illustrate the effect of the secondary cooling on the undercooling calculations, Figures 11a and 11b present the extent of the undercooled region when both standard and sharp secondary coolings are considered respectively. In the latter case, the position of the solidification front is higher in the casting machine than with the standard cooling.

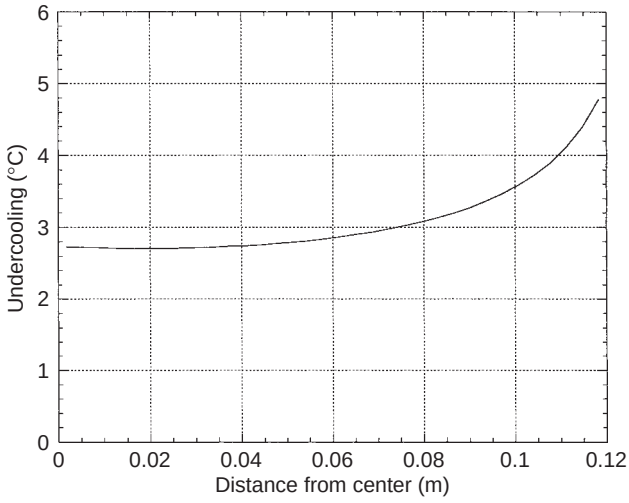

Figure 12.
Dendrite tip undercooling with sharp secondary cooling

As shown in Figure 11, the extent of the undercooled region with the sharp cooling is narrower than with the standard cooling. In these conditions, equiaxed grains are more likely to develop in the latter case and the equiaxed zone will be reduced when a sharp cooling is applied. These tendencies were experimentally observed in previous studies (Ameling *et al.*, 1986; Etienne, 1991).

7. Conclusion

The present work is a preliminary step towards the modelling of the coupled columnar and equiaxed growths in continuous casting of steel. In order to model the columnar-to-equiaxed transition in continuous casting of steel, it is necessary to take into account the undercooling at the dendrite tips. In this study, a 2-D model has been developed in order to take into account the influence of the columnar dendritic growth on heat transfer in continuous casting of steel. The model couples a classical macroscopic heat transfer model with a model of microsegregation and solutal undercooling on a microscopic scale.

The model was first applied to show the influence of the undercooling on the thermal and mass fraction fields. Results show that the calculated depth of the liquid pool is higher in the case of coupled heat transfer and undercooling calculations than obtained without taking into account the influence of the dendritic growth on heat transfer. The dendrite tip undercooling is found to be between 3 K and 5 K with standard cooling conditions. The model has also been used to study the influence of the secondary cooling on the extent of the undercooled region. When sharp secondary cooling is applied below the mould, a marked effect is observed. The undercooled region is narrower than when standard secondary cooling is applied. The application of a sharp secondary cooling can lead to a reduction of the central equiaxed region as has been observed experimentally.

References

Aboutalebi, M.R., Hassan, M. and Guthrie, R.I.L. (1995), "Coupled turbulent flow, heat transfer, and solute transport in continuous casting process", *Metall. Trans B*, 26B, 731.

Alberny, R. and Birat, J.P. (1976), "Electromagnetic stirring and quality of products", *International Conf. on Continuous Casting*, Biaritz, 140.

Ameling, D., Litterscheidt, H., Schwerdtfeger, K. and Senk, D. (1986), "Effects of sharp cooling on the structure and macrosegregation of continuously cast billets", *Steelmaking Conf. Proc.*, 387.

Ananth, R. and Gill, W.N. (1991), "A self-consistent theory of dendritic growth with convection", *J. Crystal Growth*, 108, 173.

Appolaire, B., Albert, V., Combeau, H. and Lesout, G. (1998), "Free growth of equiaxed crystals settling in undercooled NH_4Cl-H_2O", *Acta. mater.*, 221, Vol. 46, I, p. 5851.

Beckermann, C. and Viskanta, R. (1993), "Mathematical modelling of transport phenomena during alloy solidification", *Appl. Mech. Rev.*, Vol. 46 No. 1, p. 1.

Bobadilla, M., Lacaze, J. and Lesoult, G. (1988), "Influence des conditions de solidification sur le déroulement de la solidification des aciers inoxydables austénitiques", *J. Crystal Growth*, 89, 53.

Combeau, H., Roch, F., Poitrault, I., Chevrier, J.Ch. and Lesoult, G. (1990), "Numerical study of heat and mass transfer during solidification of steel ingots", in Wrobel, L.C. (Ed.), *Heat Transfer 90*, Springer Verlag, 3, 79.

Etienne, A. (1990), "Columnar and equiaxed dendrite growth in continuously cast products", *Steel Research*, Vol. 61 No. 10, p. 472.

Etienne, A. (1991), "Effects of the secondary cooling on the internal structure of blooms and billets", *1st European Conf. on Continuous Casting*, 1577.

Flint, P.J. (1990), "A three-dimentional finite difference model of heat transfer, fluid flow and solidification in the continuous slab caster", *Steelmaking Conf.*, 481.

Flood, S.C. and Hunt, J.D. (1987), "Columnar and equiaxed growth. I. A model of a columnar front with a temperature dependent velocity", *J. Crystal Growth*, 82, 543.

Ganesan, S. and Poirier, D.R. (1990), "Conservation of mass and momentum for the flow of interdendritic liquid during solidification", *Metall. Trans B*, 21B, 173.

Giovanola, B. and Kurz, W. (1990), "Modelling of microsegregation under rapid solidification conditions", *Metal. Trans. A.*, 21, 260.

Glicksman, M.E., Koss, M.B., Bushnell, L.T., Lacombe, J.C. and Winsa, E.A. (1995), "Dendritic growth of succinonitrile in terrestrial and microgravity conditions as a test of theory", *ISIJ International*, 35, 604.

Howe, H.M. (1988), "Estimation of liquidus temperatures for steels", *Iron making and Steel making*, Vol. 15 No. 3, p. 136.

Huang, X., Thomas, B.G. and Najjar, F.M. (1992), "Modeling of superheat removal during continuous casting of steel slabs", *Metall. Trans B*, 23B, 339.

Hunt, J.D. (1984), "Steady state columnar and equiaxed growth of dendrites and eutectic", *Mater. Sci. Engineer*, 65, 75.

Ivantsov, G.P. (1947), *Doherty Akademii Nauk SSSR 58*, 567.

Jang, J. and Hellawell, A. (1991), "Use of NH_4Cl-H_2O analogue casting to model aspects of continuous casting: Part 2 Columnar-equiaxed grain transition and crystal sedimentation rates", *Ironmaking and Steelmaking*, Vol. 18 No. 4, p. 275.

Kattner, U.R., Boettinger, W.J. and Coriell, S.R. (1996), "Application of Lukas' phase diagram programs to solidification calculations of multicomponent alloys", *Z. Metallkd.*, 87, 7.

Kurz, W. and Fisher, D.J. (1981), "Dendrite growth at the limit of stability: tip radius and spacing", *Acta mater.*, 29, 11.

Kurz, W. and Fisher, D.J. (1989), *Fundamentals of Solidification*, Trans Tech Publ., Aedermannsdorf.

Kurz, W., Giovanola, B. and Trivedi, R. (1986), "Theory of microstructural development during rapid solidification", *Acta mater.*, 34, 823.

Langer, J.S. and Müller-Krumbhaar (1988), "Stability effects in dendritic crystal growth", *J. Crystal Growth*, 42, 11.

M'Hamdi, M., Combeau, H., Bobadilla, M. and Lesoult, G. (1997), "Numerical modelling of heat transfer coupled with dendrite growth phenomena in continuous casting of steel", in Lewis, R.W. and Cross, J.T. (Eds), *Numerical Methods in Thermal Problems*, Vol. X, Pineridge Press, Swansea, UK, p. 435.

McCarthy, J.F. and Blake, N.W. (1996), "A front tracking model for the rapid solidification of dendritic alloys", *Acta. mater.*, 44, 2093.

Moukassi, M. (1990), "Influence du brassage du métal liquide sur le déroulement de la solidification des alliages métalliques. Application à la formation de la zone équiaxe en coulée continue", PhD thesis, INPL, France.

Ni, J. and Beckermann, C. (1991), "A volume-averaged two-phase model for transport phenomena during solidification", *Metall. Trans B*, Vol. 22B, 349.

Patankar, S.V. (1980), *Numerical Heat Transfer and Fluid Flow*, Hemisphere, New York, NY.

Sekerka, R.F., Coriell, S.R. and McFaddenn, G.B. (1995), "Stagnant film model of the effect of natural convection on the dendrite operating state", *J. Crystal Growth*, 154, 370.

Trivedi, R. (1980), "Theory of dendritic growth during the directional solidification of binary alloys", *J. Crystal Growth*, 49, 1980, 219.

Vannier, I. (1994), "Modélisation de la solidification des lingots d'acier", PhD Thesis, INPL, France.

Voller, V.R. and Prakash, G. (1987), "A fixed grid numerical modelling methodology for convection-diffusion mushy region phase-change problems", *Int. J. Heat Mass Transfer*, 30, 1709.

Wang, C.Y. and Beckermann, C. (1994), "Prediction of columnar to equiaxed transition during diffusion-controlled dendritically solidification", *Metall. Trans A*, 25A, 1081.